

Degradable ZnS-Supported Bioorthogonal Nanozymes with Enhanced Catalytic Activity for Intracellular Activation of Therapeutics

Xianzhi Zhang,[⊥] Shichao Lin,[⊥] Rui Huang, Aarohi Gupta, Stefano Fedeli, Roberto Cao-Milán, David C. Luther, Yuanchang Liu, Mingdi Jiang, Gengtan Li, Brayan Rondon, Hui Wei, and Vincent M. Rotello*

Cite This: *J. Am. Chem. Soc.* 2022, 144, 12893–12900

Read Online

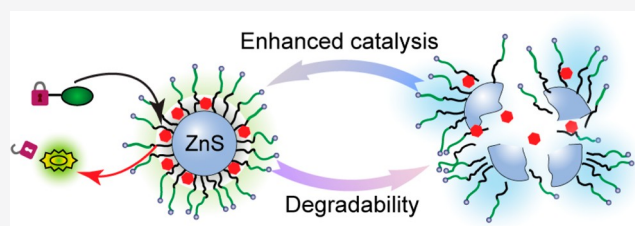
ACCESS |

Metrics & More

Article Recommendations

Supporting Information

ABSTRACT: Bioorthogonal catalysis using transition-metal catalysts (TMCs) provides a toolkit for the *in situ* generation of imaging and therapeutic agents in biological environments. Integrating TMCs with nanomaterials mimics key properties of natural enzymes, providing bioorthogonal “nanozymes”. ZnS nanoparticles provide a platform for bioorthogonal nanozymes using ruthenium catalysts embedded in self-assembled monolayers on the particle surface. These nanozymes uncage allylated profluorophores and prodrugs. The ZnS core combines the non-toxicity and degradability with the enhancement of Ru catalysis through the release of thiolate surface ligands that accelerate the rate-determining step in the Ru-mediated deallylation catalytic cycle. The maximum rate of reaction (V_{\max}) increases ~2.5-fold as compared to the non-degradable gold nanoparticle analogue. The therapeutic potential of these bioorthogonal nanozymes is demonstrated by activating a chemotherapy drug from an inactive prodrug with efficient killing of cancer cells.



INTRODUCTION

Bioorthogonal chemistry uses abiotic chemical reactions as tools for biological and biomedical applications.^{1–4} Bioorthogonal catalysis *via* transition-metal catalysts (TMCs) provides *in situ* continuous generation of imaging and therapeutic agents using transformations that cannot be accomplished by natural enzymes.^{5–9} However, the direct use of “naked” TMCs faces difficulties including poor water solubility, low stability, and lack of biocompatibility.^{10,11} In particular, TMCs are generally very sensitive to the presence of serum proteins, limiting their utility in biological and biomedical applications.^{12,13} Incorporating TMCs into nanomaterials provides bioorthogonal “nanozymes” that feature enhanced solubility, stability, and biocompatibility.^{14–18} The resulting nanozymes can activate therapeutics and imaging agents *in situ* from inactive precursors, providing on-demand “drug factories” for therapeutic applications including anticancer,^{19–27} antimicrobial,^{28,29} and anti-inflammatory treatments.³⁰

Non-degradable nanomaterials, including gold nanoparticles^{11–14,29,31,32} and polystyrene microparticles,^{19,23,33–39} are commonly used as supports for bioorthogonal nanozymes. The lack of biodegradability of these scaffolds raises concerns for bioaccumulation and long-term toxicity.⁴⁰ Degradable scaffolds have the potential to increase the ultimate biocompatibility of nanozymes. As an example, Weissleder and Miller *et al.* used biodegradable poly(lactic-*co*-glycolic acid) (PLGA) polymeric

nanoparticles to encapsulate palladium (Pd) catalysts and established anticancer therapy through activation of prodrugs.^{26,27}

Inorganic nanomaterials offer versatile platforms for bioorthogonal nanozymes, with control of structure and properties provided through engineering of the surface functionalization.⁴¹ Zinc-based nanoparticles feature biodegradability and high biocompatibility.⁴² We report here the use of zinc sulfide nanoparticles (ZnS_NP) to formulate nanozymes (ZnS_NZ) through the encapsulation of ruthenium TMCs^{13,43} inside the monolayer (Figure 1a). Significantly, the degradation process enhanced bioorthogonal catalysis in solution and in cells by the release of thiolate surface ligands (Figure 1b,c). The therapeutic potential of ZnS_NZ was demonstrated by the activation of mitoxantrone, an anticancer drug. ZnS_NZ provided more efficient eradication of cancer cells compared to comparable gold nanoparticle-based nanozymes (Au_NZ) at similar catalyst levels. Taken together, this study demonstrated the integration of biocompatible degradable nanozymes with enhanced

Received: April 28, 2022

Published: July 5, 2022



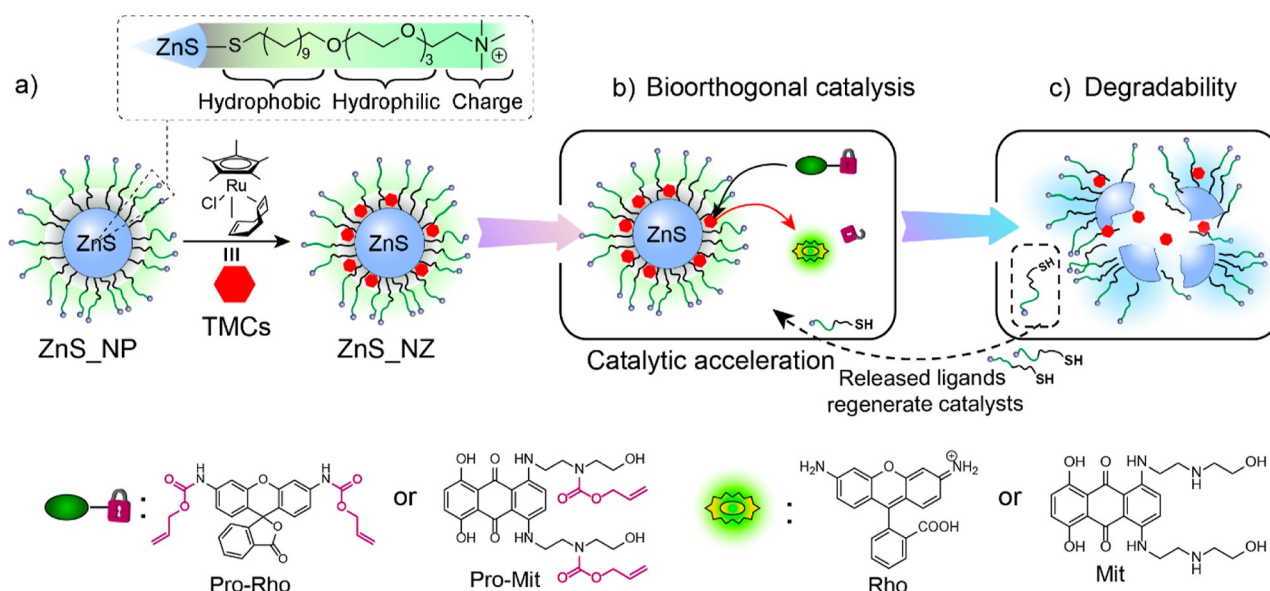


Figure 1. Schematic presentation of (a) generation of zinc sulfide nanozymes (**ZnS_NZ**) from zinc sulfide nanoparticles (**ZnS_NP**) and structures of substrates (**pro-Rho** and **pro-Mit**) and products (**Rho** and **Mit**), (b) catalytic acceleration of **ZnS_NZ**, and (c) degradability of the zinc sulfide platform.

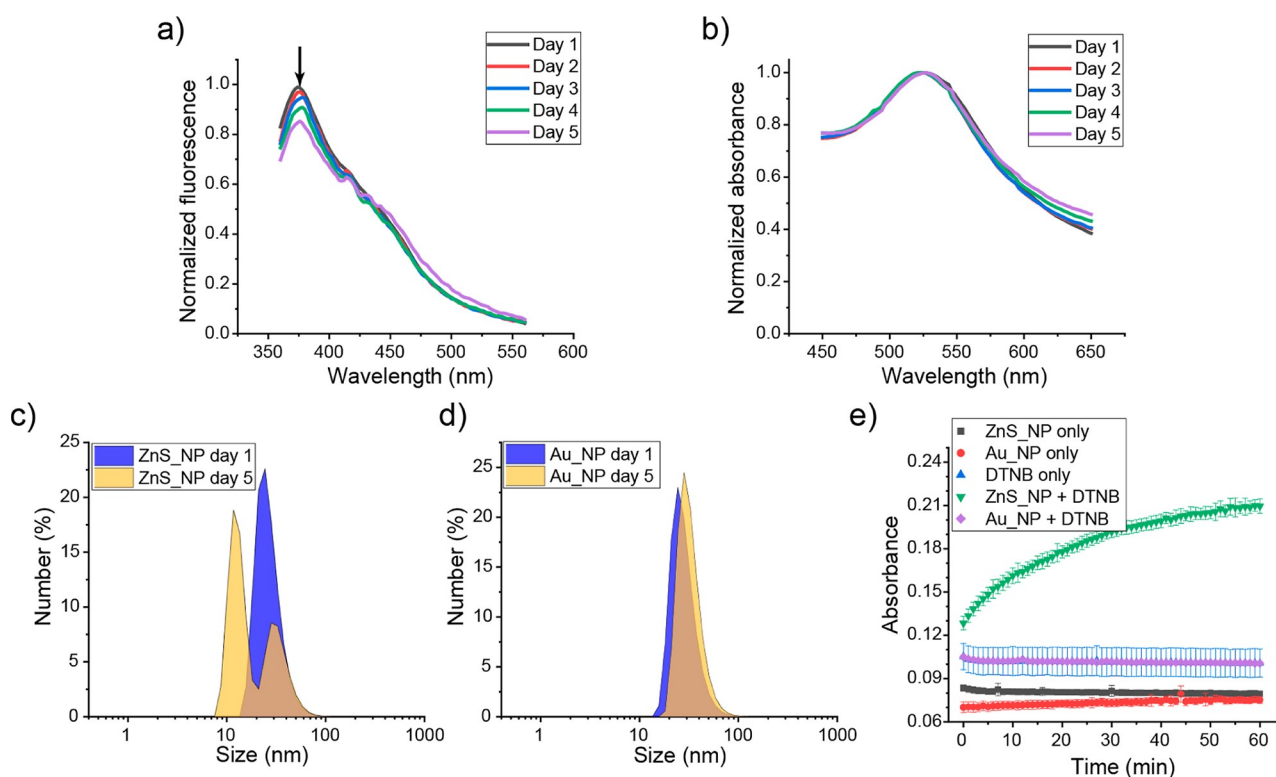


Figure 2. (a) Normalized fluorescence of 100 nM **ZnS_NP** in deionized water at 37 °C in the dark ($\lambda_{ex} = 265$ nm, $\lambda_{em} = 360-560$ nm). The decrease in fluorescence indicates the degradation of **ZnS_NP**. (b) Normalized absorbance spectra of 20 nM **AuNP** in deionized water at 37 °C in the dark indicating minimal degradation. (c,d) Size distribution of **ZnS_NP** (c) and **Au_NP** (d) before and after incubation for 5 days. (e) Absorbance at 412 nm of nanoparticles (20 nM) reacted with 0.1 mM Ellman's reagent (**DTNB**). The increased absorbance of **ZnS_NP** + **DTNB** mirrored the release of thiolate ligands (Figure S5) during the degradation. $N = 3$, mean \pm SD shown.

bioorthogonal catalysis through mechanism-based acceleration of catalysis *via* controlled nanoparticle degradation.

RESULTS AND DISCUSSION

ZnS_NP and **Au_NP** nanozymes were fabricated with a core diameter of ~ 15 nm (Figure S1, Supporting Information for NP

fabrication) and functionalized with identical cationic ligands. The resulting surface monolayer ligand features three crucial components: (1) a hydrophobic aliphatic chain to stabilize nanoparticles and encapsulate catalysts; (2) a tetra(ethylene glycol) spacer to provide biocompatibility; and (3) a quaternary

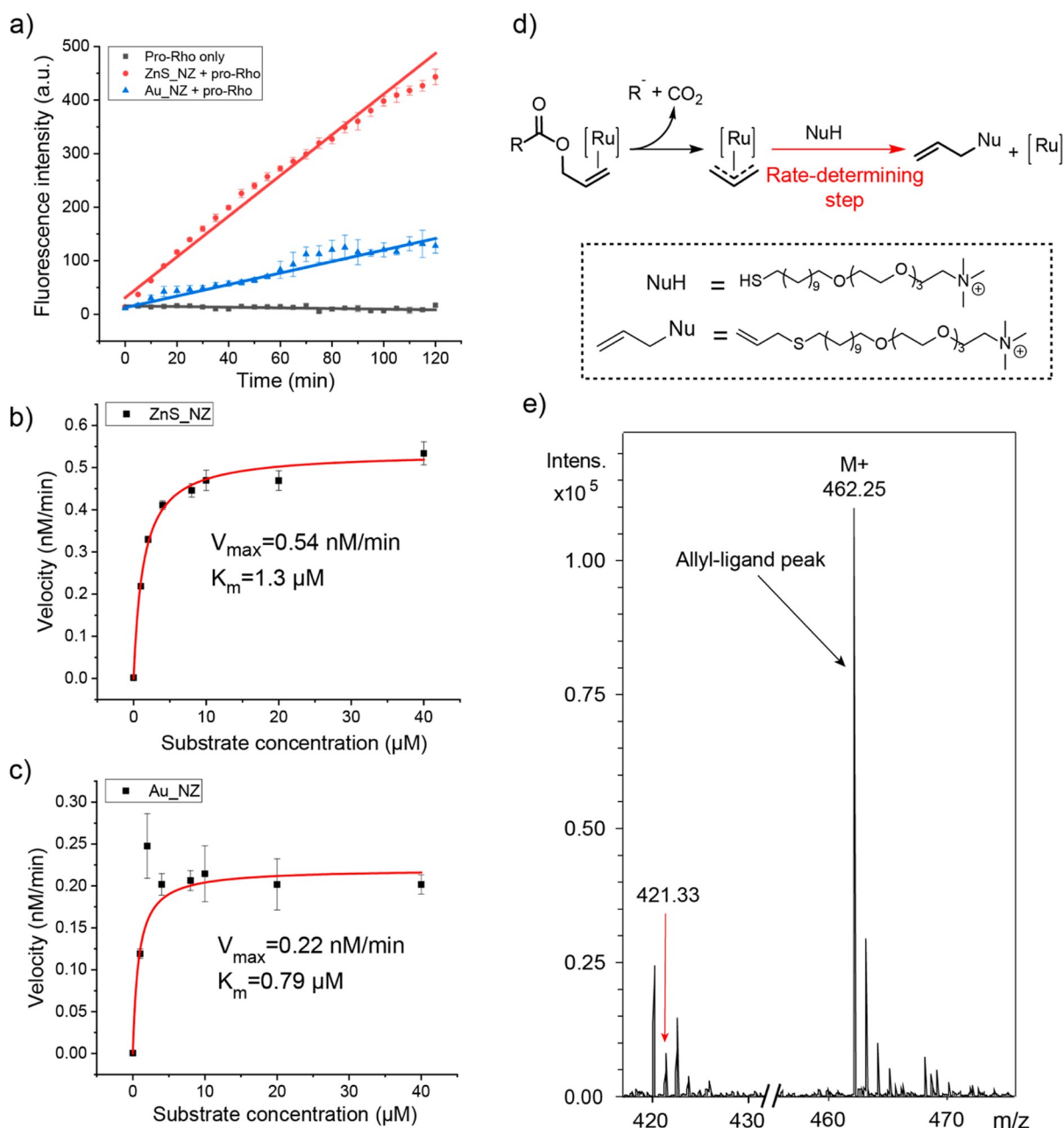


Figure 3. (a) Kinetic study of 5 nM nanozymes with 10 μM pro-Rho in PBS at 37 $^{\circ}\text{C}$. (b,c) Michaelis–Menten kinetics of 5 nM nanozymes. ZnS_NZ showed ~ 2.5 -fold enhancement in catalytic activity. Each data point represents the average of three replicates. Error bar stands for the standard deviation. (d) Proposed mechanism for deallylation reaction using the Ru catalyst. Thiols that were released from ZnS served as strong nucleophiles (Nu) and accelerated the rate-determining step of the catalytic cycle. (e) ESI-MS spectrum after ZnS_NZ-mediated decaying of pro-Rho. The free ligands (m/z 421) were converted to the allylated ligand (m/z 462). The full spectrum is presented in Figure S13.

ammonium headgroup for enhanced water solubility and cell penetration (Figures 1a, S2 and 3).

The degradability of nanoparticles was quantified through changes in the optical spectra and size distribution. ZnS_NP and Au_NP were incubated in deionized water at 37 $^{\circ}\text{C}$ in the dark for 5 days. As shown in Figure 2a, $\sim 20\%$ decrease in fluorescence was observed for ZnS_NP, suggesting the degradation of ZnS_NP. Au_NP, however, did not degrade under the same conditions, as evidenced by the negligible change in the surface plasmon resonance band (Figure 2b). The size distributions of ZnS_NP and Au_NP before and after the incubation were consistent with the optical spectra (Figure 2c,d). The size distribution of ZnS_NP changed from monomodal to bimodal

(Figure 2c), indicating that small particles were generated during the degradation, followed by the formation of agglomerates *via* flocculation and coalescence processes. In contrast, Au_NP exhibited minimal changes in the particle size and size distribution (Figure 2d), demonstrating particle stability. Research suggests that the presence of oxidants leads to the dissolution of ZnS.⁴⁴ We then incubated ZnS_NP under a nitrogen atmosphere and with hydrogen peroxide, respectively. As expected, ZnS_NP in a nitrogen environment had a minimal size change, while ZnS_NP incubated with hydrogen peroxide degraded significantly (Figure S4).

We hypothesized that the changes in the ZnS_NP size were first induced by the detachment of surface ligands. The release of

thiolate surface ligands was tracked using Ellman's reagent (*S,S'*-dithiobis-(2-nitrobenzoic acid), DTNB). In the presence of free thiols, DTNB reacts with thiols to generate a yellow-colored product. Both ZnS_NP and Au_NP (20 nM) were mixed with 0.1 mM DTNB, and the absorbance was measured at 412 nm. A continuous increase of absorbance was observed for ZnS_NP + DTNB, while almost constant absorbance was found in the control groups (Figure 2e). The release of ligands from ZnS_NP was further studied using electrospray ionization mass spectrometry (ESI-MS). ZnS_NP was incubated in deionized water at 37 °C for 3 days, and the resulting solution was lyophilized and resuspended in methanol for ESI-MS. A peak representing oxidized ligands (disulfides) was observed (Figure S5), verifying the release of surface ligands during the degradation of ZnS_NP.

Bioorthogonal nanozymes were generated by encapsulating a ruthenium-based TMC [Cp*Ru(cod)Cl] (Cp* = pentamethylcyclopentadienyl, cod = 1,5-cyclooctadiene) into the monolayers of ZnS_NP and Au_NP to generate ZnS_NZ and Au_NZ, respectively. The encapsulation of the Ru catalyst for both nanozymes was quantified by inductively coupled plasma mass spectrometry (ICP-MS), with 1300 ± 100 catalyst molecules per ZnS_NZ and 1400 ± 200 Ru per Au_NZ (Supporting Information, Table S1). The TEM and DLS (Figures S6 and 7) confirmed ZnS_NZ and Au_NZ did not show any aggregation after encapsulation. The release of catalysts from nanozymes in water was tracked for 5 days. Au_NZ had the negligible release of the catalyst, while ZnS_NZ, surprisingly, released less than 2% of the total catalyst (Figure S8).

The catalytic activity of nanozymes was quantified by the uncaging of Rhodamine-based prodrug **pro-Rho** (synthesis in Supporting Information, Figures S9 and 10). Ruthenium catalysts specifically cleave the allyloxycarbonyl groups of **pro-Rho**,⁴³ with fluorogenesis allowing quantification of the catalytic activity of the nanozymes from the calibration curve of rhodamine (Figure S11). As shown in Figure 3a, fluorescence increased after mixing nanozymes (5 nM) with **pro-Rho** (10 μ M), indicating both ZnS_NZ and Au_NZ were active. Notably, ZnS_NZ showed ~ 2.5 -fold enhancement in catalysis relative to Au_NZ. Significantly, the physiological oxidant level had a negligible influence on the catalytic activity of nanozymes (Figure S12). The same enhancement was also exhibited for the V_{\max} value (0.54 nM/min for ZnS_NZ and 0.22 nM/min for Au_NZ) and the k_{cat} value (0.11/min and 0.044/min for ZnS_NZ and Au_NZ, respectively) from the Michaelis-Menten kinetic model (Figure 3b,c). Moreover, K_m increased ~ 2 -fold for ZnS_NZ relative to Au_NZ.

We next probed the mechanistic origin for the increase in catalytic efficiency of ZnS_NZ relative to Au_NZ. Meggers *et al.* reported that the transfer of the allyl group from Ru catalysts to nucleophiles is the rate-determining step in the deallylation catalytic cycle (Figure 3d).⁴⁵ Therefore, good nucleophiles (including thiols) enhance the rate of this step and hence the overall catalytic efficiency of uncaging.⁴⁶ Based on these findings, we hypothesized that the acceleration of ZnS_NZ was due to the release of thiolate ligands during the ZnS degradation (Figure 3d). To support our hypothesis, we incubated ZnS_NZ with **pro-Rho** in PBS at 37 °C for 48 h with continuous shaking. The mixture was then lyophilized and resuspended in methanol for ESI-MS. As shown in Figures 3e and S13, the peak at 462 (*m/z*) indicates that the allyl group on the **pro-Rho** has transferred to the thiol ligand. Moreover, the

peak representing the oxidized disulfide ligand (*m/z* 421) was not significantly presented, indicating that the detached thiol ligands were allylated. This result indicates that thiol ligands were released from ZnS and participated in the ruthenium catalytic cycle.

Having characterized the catalytic activity in solution, we investigated the ability of nanozymes to uncage **pro-Rho** in living cells. HeLa cells were incubated with different concentrations of ZnS_NZ and Au_NZ nanozymes in the culture medium for 24 h to evaluate their cytotoxicity. Despite the same surface functionality and size, Au_NZ exhibited significantly higher toxicity than ZnS_NZ (Figure 4). Based on

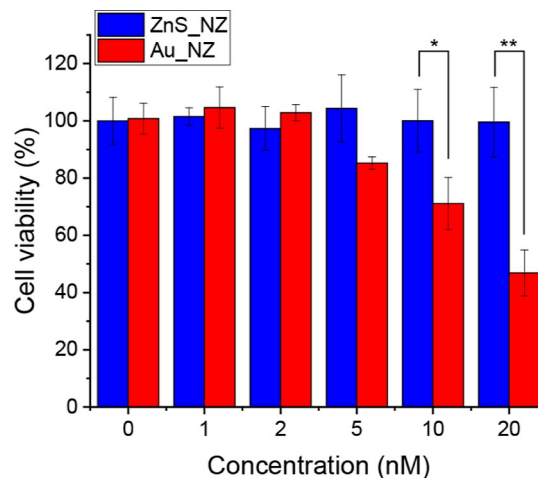


Figure 4. Cytotoxicity of ZnS_NZ and Au_NZ. ZnS_NZ exhibited significantly less toxicity than Au_NZ. Data are presented as mean \pm standard deviation, $n = 3$. *: $0.01 < p < 0.05$; **: $0.001 < p < 0.01$; and ***: $p < 0.001$.

these toxicity data, a 5 nM nanozyme concentration was used for further cell studies. The cellular internalization of nanozymes was measured by tracking Ru using ICP-MS after 24 h incubation. ZnS_NZ showed slightly lower cellular levels than Au_NZ, possibly due to the degradation of ZnS_NZ (Figure S14). For the **pro-Rho** activation study, HeLa cells were treated with nanozymes for 24 h and washed with PBS to remove excess nanozymes. Fresh media containing **pro-Rho** (100 μ M) was added to the cells for another 24 h, and the activation of **pro-Rho** in cells was imaged using confocal microscopy, with the intracellular fluorescence quantified using ImageJ software. As displayed in Figure 5a, cells treated with nanozymes exhibited green fluorescence, while the negative control (**pro-Rho** only) showed a negligible signal. This result verified the ability of nanozyme' to perform bioorthogonal catalysis in cells. Importantly, ZnS_NZ-treated cells showed ~ 2.5 -fold brighter fluorescence than Au_NZ from the confocal image (Figure 5a) and the quantification (Figure 5b). Flow cytometry analysis of fluorescence ($>10,000$ cells/condition) provided results consistent with the confocal data (Figure 5c), confirming the enhancement of catalysis in living cells by the ZnS nanoparticle scaffold.

We next explored the use of bioorthogonal ZnS_NZ for prodrug activation. A mitoxantrone (Mit) prodrug (**pro-Mit**) was used to evaluate the *in vitro* anticancer effect of nanozymes. The **pro-Mit** was synthesized by caging the pharmacophore of Mit with allyloxycarbonyl groups (synthesis in Supporting Information, Figures S15 and 16).²¹ The toxicity of **pro-Mit** was

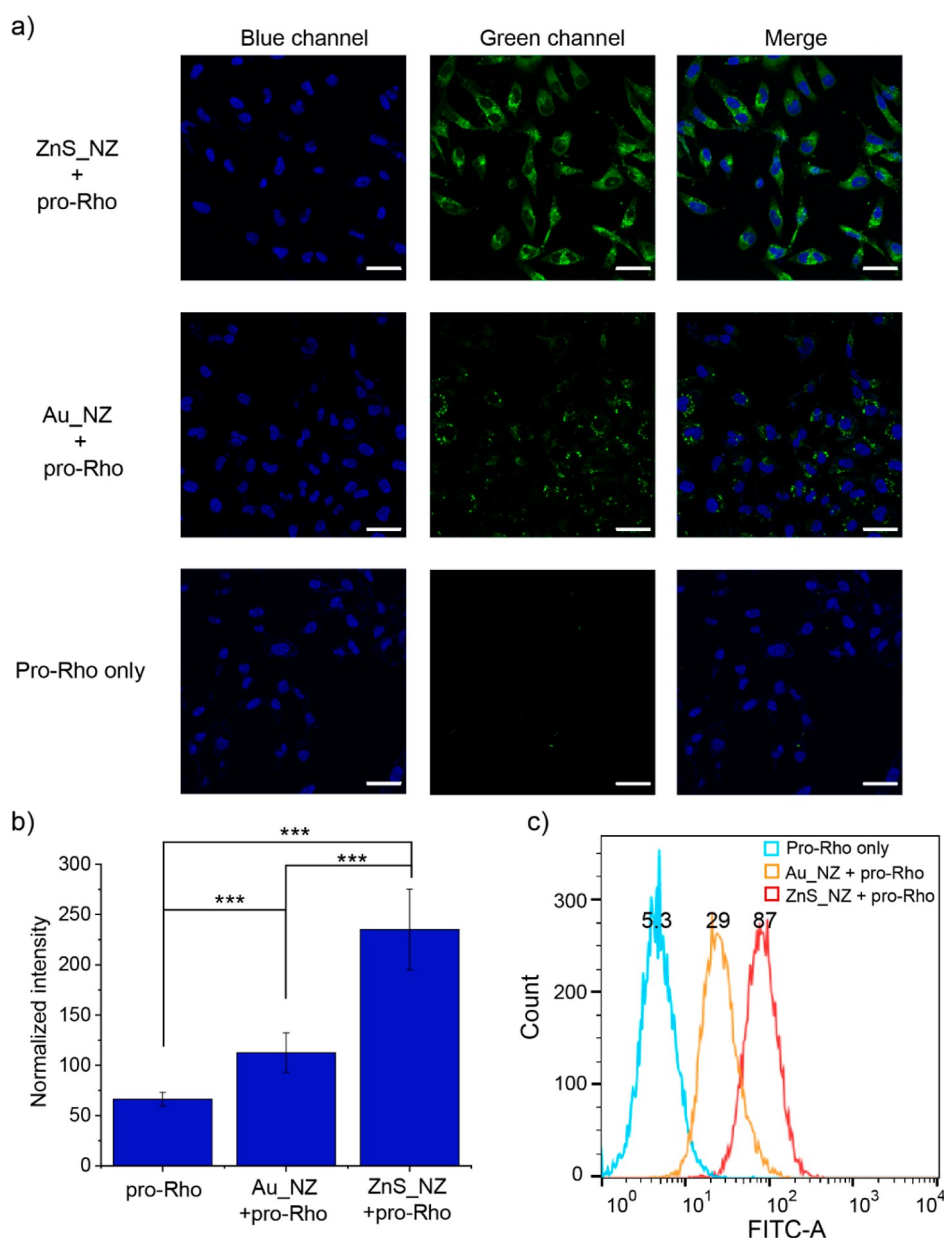


Figure 5. (a) Confocal images of HeLa cells incubated with nanozymes (5 nM), followed by the addition of **pro-Rho** (100 μ M) for 24 h. The nucleus was stained by Hoechst 33342. Scale bar = 50 μ m. (b) Quantification of intracellular fluorescence intensity by ImageJ software. Intracellular fluorescence from **ZnS_NZ**-treated cells displayed \sim 2.5-fold higher intensity than **Au_NZ**-treated ones. *: $0.01 < p < 0.05$; **: $0.001 < p < 0.01$; and ***: $p < 0.001$. (c) Flow cytometry of cells treated with **pro-Rho** only, **Au_NZ + pro-Rho**, and **ZnS_NZ + pro-Rho**. The means of three groups were 5.3, 29, and 87 a.u., respectively.

reduced more than 20-fold compared to **Mit** (Figure S17). After incubation with nanozymes, **pro-Mit** was converted to active **Mit** (Figures 6a and S18). HeLa cells were treated with nanozymes (5 nM) for 24 h, followed by **pro-Mit** (0–5 μ M) for another 24 h. Compared with **pro-Mit** only, elevated toxicity was observed in the presence of nanozymes and **pro-Mit** (Figure 6b), emphasizing the effective killing of cancer cells. Significantly, **ZnS_NZ** induced better cancer cell eradication and apoptosis (Figure S19) than **Au_NZ** presumably because of the enhanced catalytic activity of **ZnS_NZ**.

CONCLUSIONS

In summary, we have developed a strategy that uses surface-functionalized ZnS nanoparticles for achieving combined

biodegradability and enhanced bioorthogonal catalysis through ligand-mediated acceleration of catalysis. In this process, released thiols serve as nucleophiles, accelerating the rate-determining step in the uncaging of allyl-caged molecules by Ru catalysts. As compared to other types of nanozymes (including FeS) that behave as enzyme mimics,^{16,17,47–49} the ZnS-supported nanozyme can employ chemical transformation that cannot be accomplished by natural enzymes. This study demonstrates that nanoscaffolds can actively participate in bioorthogonal catalysis as a cofactor rather than simply passively encapsulating the catalysts. The superior activity relative to non-degradable gold nanoparticle nanozymes was demonstrated through the fluorophore and drug release *in vitro*, underlining the significance for biomedical applications. Overall, ZnS nanozymes offer a biocompatible platform for the safe and

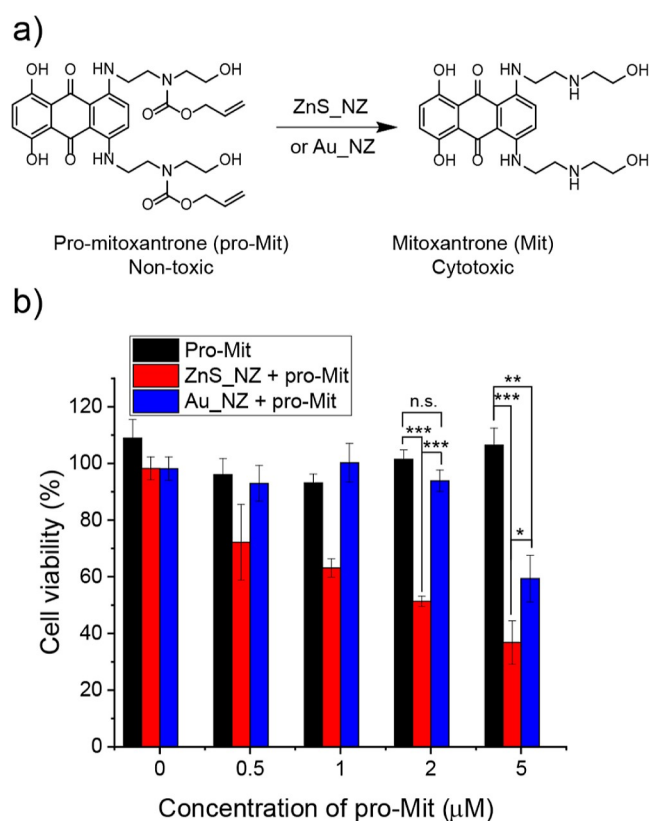


Figure 6. (a) Activation of prodrug (**pro-Mit**) by nanozymes. (b) Cell viability of HeLa cells incubated with 5 nM nanozymes, followed by treatment with prodrug (24 h). The average cell viability was measured from three replicates, and the error bars represented the standard deviation. n.s.: $0.05 < p$; *: $0.01 < p < 0.05$; **: $0.001 < p < 0.01$; and ***: $p < 0.001$.

efficient production of imaging and therapeutic agents *in situ*, promoting the clinical translation of bioorthogonal catalysis. Medical treatments featuring bioresorbable nanozymes can be safely implemented in living systems, providing localized therapies with minimal side effects. The biodegradability of the materials also avoids the risk of particle accumulation. Taken together, ZnS nanoparticles integrate biodegradability and enhanced catalytic activity, providing promising bioorthogonal nanozymes for biomedical applications.

EXPERIMENTAL SECTION

Thiol Detection. The release of thiols was detected by following the previous report using Ellman's reagent.^{50,51} Briefly, DTNB was dissolved in 0.1 M phosphate buffer containing 1 mM EDTA to obtain the stock solution. Then, 100 μL solution containing 20 nM nanoparticles and 0.1 mM DTNB were added into a 96-well clear plate and tracked the absorbance at 412 nm at 37 °C using a Molecular Devices SpectraMax M2 plate reader for 1 h.

Encapsulation of Ru into the Monolayer of Nanoparticles. The ruthenium catalyst (2 mg) was dissolved in 0.5 mL acetone and added to an 8 mL aqueous solution of nanoparticles. The solution was applied with ultracentrifugation eight times to remove the excess catalysts to obtain the corresponding nanozymes.

Kinetic Study of Nanozymes. In a 96-well black plate, **pro-Rho** solution (10 μL, 100 μM) was added, followed by adding 90 μL nanozymes solution in PBS to make the final solution containing 10 μM **pro-Rho** and 5 nM nanozymes. **Pro-Rho** alone was used as the negative control. For the Michaelis–Menten kinetic study, a solution containing nanozymes (5 nM) and **pro-Rho** (0, 1, 2, 4, 8, 10, 20, and 40 μM) was added in a 96-well black plate. The kinetic results were obtained by

tracking the fluorescence (λ_{ex} : 488 nm, λ_{em} : 521 nm, cutoff: 515 nm) using a Molecular Devices SpectraMax M2 plate reader at 37 °C for 2 h continuously.

Pro-Rho Activation in Living Cells by Nanozymes. HeLa cells were seeded at 150k in the confocal dish or 200k per well in a 6-well plate one night prior to the confocal imaging experiment or flow cytometry, respectively. Cells were treated with 5 nM **ZnS_NZ** or **Au_NZ** for 24 h, followed by multiple washings to remove the excess nanozymes. Then, fresh media containing 100 μM **pro-Rho** were incubated with cells for another 24 h. Cells were washed with PBS three times. For the confocal study, cells were stained using Hoechst 33342, washed with PBS, and imaged under a Nikon A1 spectral detector confocal microscope (A1SP) using a 40X objective. For flow cytometry, cells were harvested and resuspended in PBS and analyzed using FACS LSR II (BD Biosciences). A total of 10,000 events per sample were analyzed.

Intracellular Activation of Pro-Mit. HeLa cells (7k) were seeded in a 96-well plate one day before the experiment. Nanozymes (5 nM) were incubated with cells for 24 h, followed by multiple washing with PBS. Fresh media containing various concentrations of **pro-Mit** (0–5 μM) were then added to the cells for another 24 h. **Pro-Mit** alone was used as the negative control. Cell viability was determined by the Alamar Blue assay using the M2 microplate reader (λ_{ex} = 560 nm, λ_{em} = 590 nm).

ASSOCIATED CONTENT

Supporting Information

The Supporting Information is available free of charge at <https://pubs.acs.org/doi/10.1021/jacs.2c04571>.

Materials; synthesis and characterization of nanomaterials, pro-Rho, and pro-Mit; and toxicity of Mit and pro-Mit (PDF)

AUTHOR INFORMATION

Corresponding Author

Vincent M. Rotello – Department of Chemistry, University of Massachusetts Amherst, Amherst, Massachusetts 01003, United States; orcid.org/0000-0002-5184-5439; Email: rotello@chem.umass.edu

Authors

Xianzhi Zhang – Department of Chemistry, University of Massachusetts Amherst, Amherst, Massachusetts 01003, United States; orcid.org/0000-0002-9585-7458

Shichao Lin – Department of Chemistry, University of Massachusetts Amherst, Amherst, Massachusetts 01003, United States; Department of Biomedical Engineering, College of Engineering and Applied Sciences, Nanjing National Laboratory of Microstructures, Jiangsu Key Laboratory of Artificial Functional Materials, Nanjing University, Nanjing, Jiangsu 210023, People's Republic of China; State Key Laboratory of Analytical Chemistry for Life Science, School of Chemistry and Chemical Engineering, Chemistry and Biomedicine Innovation Center (ChemBIC), Nanjing University, Nanjing, Jiangsu 210023, People's Republic of China; Present Address: MOE Key Laboratory of Spectrochemical Analysis and Instrumentation, Key Laboratory for Chemical Biology of Fujian Province, Department of Chemical Biology, College of Chemistry and Chemical Engineering, Xiamen University, Xiamen 361005, China; orcid.org/0000-0003-3423-6225

Rui Huang – Department of Chemistry, University of Massachusetts Amherst, Amherst, Massachusetts 01003, United States; orcid.org/0000-0002-1535-9804

Aarohi Gupta – Department of Chemistry, University of Massachusetts Amherst, Amherst, Massachusetts 01003, United States; orcid.org/0000-0003-1303-1159

Stefano Fedeli – Department of Chemistry, University of Massachusetts Amherst, Amherst, Massachusetts 01003, United States

Roberto Cao-Milán – Department of Chemistry, University of Massachusetts Amherst, Amherst, Massachusetts 01003, United States

David C. Luther – Department of Chemistry, University of Massachusetts Amherst, Amherst, Massachusetts 01003, United States; orcid.org/0000-0002-4697-8683

Yuanchang Liu – Department of Chemistry, University of Massachusetts Amherst, Amherst, Massachusetts 01003, United States

Mingdi Jiang – Department of Chemistry, University of Massachusetts Amherst, Amherst, Massachusetts 01003, United States; orcid.org/0000-0002-4742-405X

Gengtan Li – Department of Chemistry, University of Massachusetts Amherst, Amherst, Massachusetts 01003, United States

Brayan Rondon – Department of Chemistry, University of Massachusetts Amherst, Amherst, Massachusetts 01003, United States

Hui Wei – Department of Biomedical Engineering, College of Engineering and Applied Sciences, Nanjing National Laboratory of Microstructures, Jiangsu Key Laboratory of Artificial Functional Materials, Nanjing University, Nanjing, Jiangsu 210023, People's Republic of China; State Key Laboratory of Analytical Chemistry for Life Science, School of Chemistry and Chemical Engineering, Chemistry and Biomedicine Innovation Center (ChemBIC), Nanjing University, Nanjing, Jiangsu 210023, People's Republic of China; orcid.org/0000-0003-0870-7142

Complete contact information is available at:
<https://pubs.acs.org/10.1021/jacs.2c04571>

Author Contributions

[†]X.Z. and S.L. contributed equally.

Notes

The authors declare no competing financial interest.

ACKNOWLEDGMENTS

This work was supported by the National Institutes of Health EB022641 and the NSF (CHE-2108044, ICP-MS). S.L. thanks the financial support from Visiting Scholar Funding of Nanjing University.

REFERENCES

- (1) Sletten, E. M.; Bertozzi, C. R. Bioorthogonal Chemistry: Fishing for Selectivity in a Sea of Functionality. *Angew. Chem., Int. Ed.* **2009**, *48*, 6974–6998.
- (2) Prescher, J. A.; Bertozzi, C. R. Chemistry in Living Systems. *Nat. Chem. Biol.* **2005**, *1*, 13–21.
- (3) Wang, J.; Wang, X.; Fan, X.; Chen, P. R. Unleashing the Power of Bond Cleavage Chemistry in Living Systems. *ACS Cent. Sci.* **2021**, *7*, 929–943.
- (4) Bird, R. E.; Lemmel, S. A.; Yu, X.; Zhou, Q. A. Bioorthogonal Chemistry and Its Applications. *Bioconjugate Chem.* **2021**, *32*, 2457–2479.
- (5) Martínez-Calvo, M.; Mascareñas, J. L. Organometallic Catalysis in Biological Media and Living Settings. *Coord. Chem. Rev.* **2018**, *359*, 57–79.

- (6) van de L'Isle, M. O. N.; Ortega-Liebana, M. C.; Unciti-Broceta, A. Transition Metal Catalysts for the Bioorthogonal Synthesis of Bioactive Agents. *Curr. Opin. Chem. Biol.* **2021**, *61*, 32–42.

- (7) Li, J.; Chen, P. R. Development and Application of Bond Cleavage Reactions in Bioorthogonal Chemistry. *Nat. Chem. Biol.* **2016**, *12*, 129–137.

- (8) Bai, Y.; Chen, J.; Zimmerman, S. C. Designed Transition Metal Catalysts for Intracellular Organic Synthesis. *Chem. Soc. Rev.* **2018**, *47*, 1811–1821.

- (9) Liu, Y.; Bai, Y. Design and Engineering of Metal Catalysts for Bio-Orthogonal Catalysis in Living Systems. *ACS Appl. Bio Mater.* **2020**, *3*, 4717–4746.

- (10) Zhang, X.; Huang, R.; Gopalakrishnan, S.; Cao-Milán, R.; Rotello, V. M. Bioorthogonal Nanozymes: Progress towards Therapeutic Applications. *Trends Chem.* **2019**, *1*, 90–98.

- (11) Tonga, G. Y.; Jeong, Y.; Duncan, B.; Mizuhara, T.; Mout, R.; Das, R.; Kim, S. T.; Yeh, Y.-C.; Yan, B.; Hou, S.; et al. Supramolecular Regulation of Bioorthogonal Catalysis in Cells Using Nanoparticle-Embedded Transition Metal Catalysts. *Nat. Chem.* **2015**, *7*, 597–603.

- (12) Zhang, X.; Liu, Y.; Gopalakrishnan, S.; Castellanos-Garcia, L.; Li, G.; Malassiné, M.; Uddin, I.; Huang, R.; Luther, D. C.; Vachet, R. W.; et al. Intracellular Activation of Bioorthogonal Nanozymes through Endosomal Proteolysis of the Protein Corona. *ACS Nano* **2020**, *14*, 4767–4773.

- (13) Zhang, X.; Fedeli, S.; Gopalakrishnan, S.; Huang, R.; Gupta, A.; Luther, D. C.; Rotello, V. M. Protection and Isolation of Bioorthogonal Metal Catalysts by Using Monolayer-Coated Nanozymes. *ChemBioChem* **2020**, *21*, 2759–2763.

- (14) Cao-Milán, R.; He, L. D.; Shorkey, S.; Tonga, G. Y.; Wang, L. S.; Zhang, X.; Uddin, I.; Das, R.; Sulak, M.; Rotello, V. M. Modulating the Catalytic Activity of Enzyme-like Nanoparticles through Their Surface Functionalization. *Mol. Syst. Des. Eng.* **2017**, *2*, 624–628.

- (15) Wang, W.; Zhang, X.; Huang, R.; Hirschbiegel, C.-M.; Wang, H.; Ding, Y.; Rotello, V. M. In Situ Activation of Therapeutics through Bioorthogonal Catalysis. *Adv. Drug Deliv. Rev.* **2021**, *176*, 113893.

- (16) Wu, J.; Wang, X.; Wang, Q.; Lou, Z.; Li, S.; Zhu, Y.; Qin, L.; Wei, H. Nanomaterials with Enzyme-like Characteristics (Nanozymes): Next-Generation Artificial Enzymes (II). *Chem. Soc. Rev.* **2019**, *48*, 1004–1076.

- (17) Huang, Y.; Ren, J.; Qu, X. Nanozymes: Classification, Catalytic Mechanisms, Activity Regulation, and Applications. *Chem. Rev.* **2019**, *119*, 4357–4412.

- (18) Fedeli, S.; Im, J.; Gopalakrishnan, S.; Elia, J. L.; Gupta, A.; Kim, D.; Rotello, V. M. Nanomaterial-Based Bioorthogonal Nanozymes for Biological Applications. *Chem. Soc. Rev.* **2021**, *50*, 13467–13480.

- (19) Weiss, J. T.; Dawson, J. C.; Macleod, K. G.; Rybski, W.; Fraser, C.; Torres-Sánchez, C.; Patton, E. E.; Bradley, M.; Carragher, N. O.; Unciti-Broceta, A. Extracellular Palladium-Catalysed Dealkylation of 5-Fluoro-1-Propargyl-Uracil as a Bioorthogonally Activated Prodrug Approach. *Nat. Commun.* **2014**, *5*, 3277.

- (20) Chen, Z.; Li, H.; Bian, Y.; Wang, Z.; Chen, G.; Zhang, X.; Miao, Y.; Wen, D.; Wang, J.; Wan, G.; et al. Bioorthogonal Catalytic Patch. *Nat. Nanotechnol.* **2021**, *16*, 933–941.

- (21) Zhang, X.; Landis, R. F.; Keshri, P.; Cao-Milán, R.; Luther, D. C.; Gopalakrishnan, S.; Liu, Y.; Huang, R.; Li, G.; Malassiné, M.; et al. Intracellular Activation of Anticancer Therapeutics Using Polymeric Bioorthogonal Nanocatalysts. *Adv. Healthcare Mater.* **2021**, *10*, 2001627.

- (22) Sancho-albero, M.; Rubio-ruiz, B.; Pérez-López, A. M.; Sebastián, V.; Martín-Duque, P.; Arruebo, M.; Santamaría, J.; Unciti-broceta, A. Cancer-Derived Exosomes Loaded with Ultrathin Palladium Nanosheets for Targeted Bioorthogonal Catalysis. *Nat. Catal.* **2019**, *2*, 864–872.

- (23) Bray, T. L.; Salji, M.; Brombin, A.; Pérez-López, A. M.; Rubio-Ruiz, B.; Galbraith, L. C. A.; Patton, E. E.; Leung, H. Y.; Unciti-Broceta, A. Bright Insights into Palladium-Triggered Local Chemotherapy. *Chem. Sci.* **2018**, *9*, 7354–7361.

- (24) Wang, F.; Zhang, Y.; Liu, Z.; Du, Z.; Zhang, L.; Ren, J.; Qu, X. A Biocompatible Heterogeneous MOF-Cu Catalyst for In Vivo Drug

- Synthesis in Targeted Subcellular Organelles. *Angew. Chem.* **2019**, *58*, 6987–6992.
- (25) Clavadetscher, J.; Indrigo, E.; Chankeshwara, S. V.; Lilienkampf, A.; Bradley, M. In-Cell Dual Drug Synthesis by Cancer-Targeting Palladium Catalysts. *Angew. Chem.* **2017**, *129*, 6968–6972.
- (26) Miller, M. A.; Mikula, H.; Luthria, G.; Li, R.; Kronister, S.; Prytykch, M.; Kohler, R. H.; Mitchison, T.; Weissleder, R. Modular Nanoparticulate Prodrug Design Enables Efficient Treatment of Solid Tumors Using Bioorthogonal Activation. *ACS Nano* **2018**, *12*, 12814–12826.
- (27) Miller, M. A.; Askevold, B.; Mikula, H.; Kohler, R. H.; Pirovich, D.; Weissleder, R. Nano-Palladium Is a Cellular Catalyst for in Vivo Chemistry. *Nat. Commun.* **2017**, *8*, 15906.
- (28) Huang, R.; Li, C.-H.; Cao-Milán, R.; He, L. D.; Makabenta, J. M.; Zhang, X.; Yu, E.; Rotello, V. M. Polymer-Based Bioorthogonal Nanocatalysts for the Treatment of Bacterial Biofilms. *J. Am. Chem. Soc.* **2020**, *142*, 10723–10729.
- (29) Cao-Milán, R.; Gopalakrishnan, S.; He, L. D.; Huang, R.; Wang, L.; Castellanos, L.; Luther, D. C.; Landis, R. F.; Makabenta, J. M. V.; Li, C.; et al. Thermally Gated Bio-Orthogonal Nanozymes with Supramolecularly Confined Porphyrin Catalysts for Antimicrobial Uses. *Chem* **2020**, *6*, 1113–1124.
- (30) Du, Z.; Liu, C.; Song, H.; Scott, P.; Liu, Z.; Ren, J.; Qu, X. Neutrophil-Membrane-Directed Bioorthogonal Synthesis of Inflammation-Targeting Chiral Drugs. *Chem* **2020**, *6*, 2060–2072.
- (31) Gupta, A.; Das, R.; Yesilbag Tonga, G.; Mizuhara, T.; Rotello, V. M. Charge-Switchable Nanozymes for Bioorthogonal Imaging of Biofilm-Associated Infections. *ACS Nano* **2018**, *12*, 89–94.
- (32) Das, R.; Landis, R. F.; Tonga, G. Y.; Cao-Milán, R.; Luther, D. C.; Rotello, V. M. Control of Intra- versus Extracellular Bioorthogonal Catalysis Using Surface-Engineered Nanozymes. *ACS Nano* **2019**, *13*, 229–235.
- (33) Yusop, R. M.; Unciti-Broceta, A.; Johansson, E. M. V.; Sánchez-Martín, R. M.; Bradley, M. Palladium-Mediated Intracellular Chemistry. *Nat. Chem.* **2011**, *3*, 239–243.
- (34) Weiss, J. T.; Dawson, J. C.; Fraser, C.; Rybski, W.; Torres-Sánchez, C.; Bradley, M.; Patton, E. E.; Carragher, N. O.; Unciti-Broceta, A. Development and Bioorthogonal Activation of Palladium-Labile Prodrugs of Gemcitabine. *J. Med. Chem.* **2014**, *57*, 5395–5404.
- (35) Weiss, J. T.; Carragher, N. O.; Unciti-broceta, A. Palladium-Mediated Dealkylation of N-Propargyl-Floxuridine as a Bioorthogonal Oxygen-Independent Prodrug Strategy. *Sci. Rep.* **2015**, *5*, 9329.
- (36) Rubio-Ruiz, B.; Weiss, J. T.; Unciti-Broceta, A. Efficient Palladium-Triggered Release of Vorinostat from a Bioorthogonal Precursor. *J. Med. Chem.* **2016**, *59*, 9974–9980.
- (37) Pérez-López, A. M.; Rubio-Ruiz, B.; Sebastián, V.; Hamilton, L.; Adam, C.; Bray, T. L.; Irusta, S.; Brennan, P. M.; Lloyd-Jones, G. C.; Sieger, D.; et al. Gold-Triggered Uncaging Chemistry in Living Systems. *Angew. Chem., Int. Ed.* **2017**, *56*, 12548–12552.
- (38) Clavadetscher, J.; Indrigo, E.; Chankeshwara, S. V.; Lilienkampf, A.; Bradley, M. In-Cell Dual Drug Synthesis by Cancer-Targeting Palladium Catalysts. *Angew. Chem., Int. Ed.* **2017**, *56*, 6864–6868.
- (39) Adam, C.; Pérez-López, A. M.; Hamilton, L.; Rubio-Ruiz, B.; Bray, T. L.; Sieger, D.; Brennan, P. M.; Unciti-Broceta, A. Bioorthogonal Uncaging of the Active Metabolite of Irinotecan by Palladium-Functionalized Microdevices. *Chem.—Eur. J.* **2018**, *24*, 16783–16790.
- (40) Luther, D. C.; Huang, R.; Jeon, T.; Zhang, X.; Lee, Y.-W.; Nagaraj, H.; Rotello, V. M. Delivery of Drugs, Proteins, and Nucleic Acids Using Inorganic Nanoparticles. *Adv. Drug Deliv. Rev.* **2020**, *156*, 188–213.
- (41) Erathodiyil, N.; Ying, J. Y. Functionalization of Inorganic Nanoparticles for Bioimaging Applications. *Acc. Chem. Res.* **2011**, *44*, 925–935.
- (42) Venezuela, J.; Dargusch, M. S. The Influence of Alloying and Fabrication Techniques on the Mechanical Properties, Biodegradability and Biocompatibility of Zinc : A Comprehensive Review. *Acta Biomater.* **2019**, *87*, 1–40.
- (43) Streu, C.; Meggers, E. Ruthenium-Induced Allylcarbamate Cleavage in Living Cells. *Angew. Chem., Int. Ed.* **2006**, *45*, 5645–5648.
- (44) Eskelsen, J. R.; Xu, J.; Chiu, M.; Moon, J.-W.; Wilkins, B.; Graham, D. E.; Gu, B.; Pierce, E. M. Influence of Structural Defects on Biomineralized ZnS Nanoparticle Dissolution: An in-Situ Electron Microscopy Study. *Environ. Sci. Technol.* **2018**, *52*, 1139–1149.
- (45) Völker, T.; Dempwolf, F.; Graumann, P. L.; Meggers, E. Progress towards Bioorthogonal Catalysis with Organometallic Compounds. *Angew. Chem., Int. Ed.* **2014**, *53*, 10536–10540.
- (46) Völker, T.; Meggers, E. Chemical Activation in Blood Serum and Human Cell Culture: Improved Ruthenium Complex for Catalytic Uncaging of Alloc-Protected Amines. *ChemBioChem* **2017**, *18*, 1083–1086.
- (47) Maji, S. K.; Dutta, A. K.; Biswas, P.; Srivastava, D. N.; Paul, P.; Mondal, A.; Adhikary, B. Synthesis and Characterization of FeS Nanoparticles Obtained from a Dithiocarboxylate Precursor Complex and Their Photocatalytic, Electrocatalytic and Biomimic Peroxidase Behavior. *Appl. Catal., A* **2012**, *419–420*, 170–177.
- (48) Dutta, A. K.; Maji, S. K.; Srivastava, D. N.; Mondal, A.; Biswas, P.; Paul, P.; Adhikary, B. Synthesis of FeS and FeSe Nanoparticles from a Single Source Precursor: A Study of Their Photocatalytic Activity, Peroxidase-Like Behavior, and Electrochemical Sensing of H₂O₂. *ACS Appl. Mater. Interfaces* **2012**, *4*, 1919–1927.
- (49) Dai, Z.; Liu, S.; Bao, J.; Ju, H. Nanostructured FeS as a Mimic Peroxidase for Biocatalysis and Biosensing. *Chem.—Eur. J.* **2009**, *15*, 4321–4326.
- (50) Sharma, S. K.; Adumeau, P.; Keinänen, O.; Sisodiya, V.; Sarvaiya, H.; Tchelepi, R.; Korsen, J. A.; Pourat, J.; Edwards, K. J.; Ragupathi, A.; et al. Synthesis and Comparative in Vivo Evaluation of Site-Specifically Labeled Radioimmunoconjugates for DLL3-Targeted ImmunoPET. *Bioconjugate Chem.* **2021**, *32*, 1255–1262.
- (51) Ellman, G. L. Tissue sulfhydryl groups. *Arch. Biochem. Biophys.* **1959**, *82*, 70–77.